Photodetachment of Gaseous Multiply Charged Anions, Copper Phthalocyanine Tetrasulfonate Tetraanion: Tuning Molecular Electronic Energy Levels by Charging and Negative Electron Binding

Xue-Bin Wang,[†,‡] Kim Ferris,*[,§] and Lai-Sheng Wang*[,†,‡]

Department of Physics, Washington State University, Richland, Washington 99352, W. R. Wiley Environmental Molecular Sciences Laboratory, Pacific Northwest National Laboratory, MS K8-88, P.O. Box 999, Richland, Washington 99352, and Materials Science Department, Pacific Northwest National Laboratory, MS K2-44, P.O. Box 999, Richland, Washington 99352

Received: August 24, 1999

We report photodetachment photoelectron spectroscopy (PES) of gaseous copper phthalocyanine (CuPc) tetrasulfonate quadruply charged anions, $[CuPc(SO_3)_4]^{4-}$, and its monoprotonated and -sodiumated triply charged anions, $[CuPc(SO_3)_4H]^{3-}$ and $[CuPc(SO_3)_4Na]^{3-}$. The $[CuPc(SO_3)_4]^{4-}$ tetraanion was found to possess a negative electron binding energy of −0.9 eV, whereas the trianions have binding energies of 1.0 and 1.2 eV for the sodiumated and protonated species, respectively. The PES spectral features of the three multiply charged anions were observed to be similar to that of the parent CuPc neutral molecule, except that the anions have lower binding energies due to the presence of the negative charges ($-SO_3^-$). The data thus suggested a stepwise tuning of the molecular electronic energy levels of the CuPc molecule through charging, wherein the molecular orbital energies of the parent molecule were systematically pushed up by the negative charges. We further carried out semiempirical calculations, which provided insight into the nature of the localized charges on the peripheral $-SO_3^-$ groups and the intramolecular electrostatic interactions in the multiply charged anions and confirmed the interpretation of the stepwise tuning of molecular energy levels by charging. Photon energy-dependent studies revealed the effects of the repulsive Coulomb barriers on the photodetachment PES spectra of the multiply charged anions. The barrier heights were estimated to be about 3.5 and 2.5 eV for the tetra- and trianions, respectively. We also observed excited states for the multiply charged anions and resonant tunneling through the repulsive Coulomb barriers via the excited states.

1. Introduction

Electrostatic charging is a common phenomenon in nature and electrostatic interactions are central in determining the structure and function of biomolecules and the chemical physical properties of materials.[1] Understanding the strength and nature of these interactions requires a detailed characterization of the individual molecular properties and solvation effects. Coulomb attraction or repulsion between charged species is screened in solution due to the dielectric effect of the solvent or protein matrix.[2] Gas-phase investigations involving multiply charged species, on the other hand, can yield information about the long-range Coulomb interactions without complications of the solvents. Solvation effects can then be quantitatively evaluated and characterized by studying solvated multiply charged species with controlled solvent numbers. Thus, investigation of gaseous multiply charged ions offers a unique opportunity to obtain molecular-level information about electrostatic interactions, as well as solvent influence on their stability.

Mass spectrometry coupled with electrospray has already been used to investigate Coulomb repulsions in multiply charged cations in the gas phase.[3−6] There have also been significant recent efforts focused on gas-phase multiply charged anions.[7−13] We have recently developed a new technique to investigate gaseous multiply charged anions using photodetachment photoelectron spectroscopy (PES) and electrospray.[14,15] PES is ideal to study the electrostatic interactions in gaseous multiply charged anions. In PES, one measures the binding energies of electrons, which carry direct information about the Coulomb repulsions in and electronic stability of multiply charged anions. PES also provides information about the electronic structure of the multiply charged anions. Performing PES at various photon energies, we have observed directly the repulsive Coulomb barrier (RCB) that exists in multiply charged species[7] and electron tunneling through the RCB in a number of doubly charged anions.[14,16−19] We have also observed solvent stabilization of doubly charged anions.[20]

In the present paper, we report a PES study of a quadruply charged gaseous anion, copper phthalocyanine (CuPc) tetrasulfonate tetraanion, $[CuPc(SO_3)_4]^{4-}$, and its monoprotonated and -sodiumated triply charged anions, $[CuPc(SO_3)_4H]^{3-}$ and $[CuPc(SO_3)_4Na]^{3-}$, at four photon energies, 193 (6.424 eV), 266 (4.661 eV), 355 (3.496 eV), and 532 (2.331 eV) nm. We present the first observation of negative electron binding in a multiply charged anion and a stepwise tuning of electronic energy levels of the parent CuPc molecule by adding negative charge groups ($-SO_3^-$) to its periphery. We show that the molecular orbital (MO) energies of the cyclic CuPc molecule are systematically pushed up (decreasing orbital binding energies) by adding $-SO_3^-$. With four $-SO_3^-$, the binding energy of the highest occupied molecular orbital (HOMO) of CuPc becomes negative

[†] Washington State University.
[‡] W. R. Wiley Environmental Molecular Sciences Laboratory, Pacific Northwest National Laboratory.
[§] Materials Science Department, Pacific Northwest National Laboratory.

10.1021/jp9930090 CCC: $19.00
Published on Web 12/09/1999

(−0.9 eV). The upward shift of the CuPc HOMO and the negative electron binding, observed through photodetachment experiments of the quadruply charged $[CuPc(SO_3)_4]^{4-}$ anion, are owing to the charge localization in $-SO_3^-$ and the Coulomb repulsion of the excess charges. The tetraanion is thus metastable against electron detachment and stores 0.9 eV excess electrostatic energy. The trianions have similar PES spectra as that of the tetraanion, except that they have higher binding energies due to the fewer negative charges. Semiempirical calculations were carried out for the parent CuPc, the monoprotonated trianion, and the tetraanion. The calculations showed clearly a rigid shifting of the MO energies for CuPc as the $-SO_3^-$ groups are attached to its periphery, consistent with the experimental observations. The localized nature of the charge in the $-SO_3^-$ groups was also shown clearly from the calculations.

A preliminary account of the observation of the negative electron-binding energy in the tetraanion has been recently reported.[21] In the current paper, we present all the experimental results, including data on the sodiumated trianion and detailed photon energy-dependent studies, as well as the semiempirical calculations. In particular, the photon energy-dependent studies revealed the effects of the RCB on the photodetachment transitions, leading to observations of two-photon processes and resonant tunneling through the RCB.

2. Experimental Section

Our experiment involved generation of gas-phase multiply charged negative ions using electrospray[22] and photodetachment photoelectron spectroscopy of size- and charge-selected anions. Details of the experiment have been described elsewhere.[15] The electrospray was started with a 10^{-4} M CuPc−3,4′,4″,4‴-tetrasulfonate sodium salt solution in a water/methanol (2:98 ratio) mixed solvent at neutral pH. The anions produced from the electrospray were accumulated and stored in a quadrupole ion trap for 0.1 s before being analyzed by a time-of-flight (TOF) mass spectrometer. The major anion signals were due to the $[CuPc(SO_3)_4]^{4-}$ tetraanion. The monoprotonated and -sodiumated trianions were also present, but with only about 10% the abundance of the tetraanion. The anions of interest were selected by a mass gate and decelerated by a momentum decelerator before being crossed by a detachment laser beam. We used four detachment photon energies ($h\nu$): 6.424 eV (193 nm) from an ArF excimer laser and the fourth (266 nm, 4.661 eV), third (355 nm, 3.496 eV), and second (532 nm, 2.331 eV) harmonics of a Nd:YAG laser. We measured the kinetic energies (KE) of the photoemitted electrons using a magnetic bottle TOF electron analyzer with nearly 100% collecting efficiency. The experiments were done at 10 Hz repetition rate at 532 and 355 nm and 20 Hz repetition rate at 193 and 266 nm with the ion beam off at alternating laser shots for background subtraction. The TOF-to-KE spectral conversions were calibrated using the known spectra of I^- and O^-. The electron binding energies (BE) were determined from Einstein's photoelectric equation, $h\nu =$ BE + KE. The energy resolution of the PES apparatus was about $\Delta KE/KE \approx 2\%$.[15]

3. Results

Figure 1 shows the PES spectra of $[CuPc(SO_3)_4]^{4-}$, $[CuPc(SO_3)_4Na]^{3-}$, and $[CuPc(SO_3)_4H]^{3-}$ at 193 nm. The spectrum of $[CuPc(SO_3)_4]^{4-}$ reveals a weak feature (X) at negative binding energies with a threshold energy of −0.9 eV and two broad features (A and B) at positive binding energies. The spectra of $[CuPc(SO_3)_4Na]^{3-}$ and $[CuPc(SO_3)_4H]^{3-}$ are nearly identical, each with three spectral features (X, A, and B), which are rather similar to those observed for $[CuPc(SO_3)_4]^{4-}$. The threshold

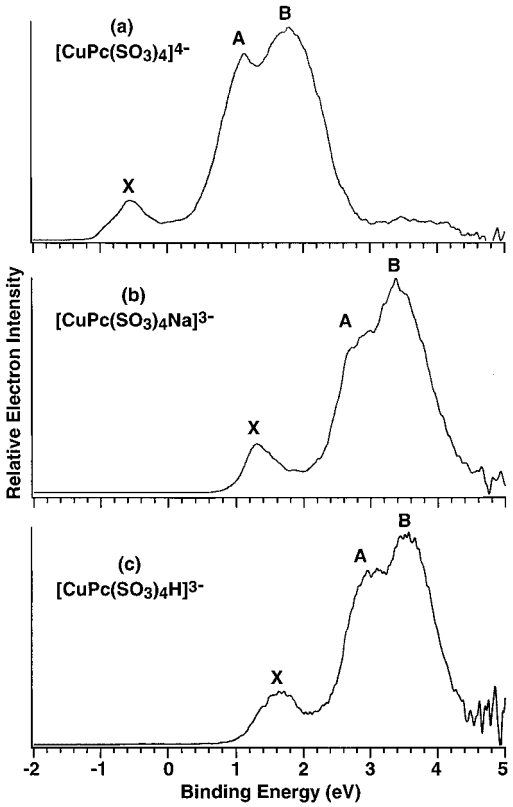

Figure 1. Photoelectron spectra at 193 nm of (a) $[CuPc(SO_3)_4]^{4-}$, (b) $[CuPc(SO_3)_4Na]^{3-}$, and (c) $[CuPc(SO_3)_4H]^{3-}$.

binding energy of $[CuPc(SO_3)_4H]^{3-}$ was measured to be 1.2 eV, slightly higher than the 1.0 eV value measured for that of $[CuPc(SO_3)_4Na]^{3-}$.

3.1. $[CuPc(SO_3)_4]^{4-}$. Figure 2 displays the spectra of $[CuPc(SO_3)_4]^{4-}$ at all the four photon energies. At 266 nm, feature B peaking at ∼2 eV completely disappeared, whereas feature A was only partially observed (Figure 2b). At 355 nm, feature A also completely disappeared, while the ground-state feature (X) was observed, but its higher BE side seemed to be cutoff. Interestingly, a weak feature (X′) at lower BE appeared in the 355 nm spectrum. The weak signals at the high BE side in the spectra of 355, 266, and 193 nm were shown to be due to detachment of the product trianion by absorption of a second photon in each case ; the relative intensities of these weak signals could be enhanced at higher detachment photon fluxes.

According to the trend of the PES spectra from 193 to 355 nm, we did not anticipate observing any signals at 532 nm. Indeed, the X feature completely disappeared in the 532 nm spectrum (Figure 2d). However, a totally unexpected and sharp feature (X″) was observed at 0.30 eV. The feature X′ observed at 355 nm also appeared in the 532 nm spectrum. To understand the nature of the X′ and X″ features, we further performed photon-flux-dependent studies, as shown in Figure 3. Surprisingly, the width of the sharp feature (X″) did not depend on the photon flux and its intensity was scaled to the photon-flux linearly. The lower BE feature (X′), on the other hand, was observed to be enhanced at high photon fluxes and it approximately scaled quadratically with the photon flux. These observations suggested that the X′ feature was due to a two-photon process, whereas the X″ feature was due to a single-photon process.

3.2. $[CuPc(SO_3)_4Na]^{3-}$. Figure 4 shows the spectra of $[CuPc(SO_3)_4Na]^{3-}$ at three photon energies. At 266 nm, feature B completely disappeared. The weak signal at ∼3.4 eV was

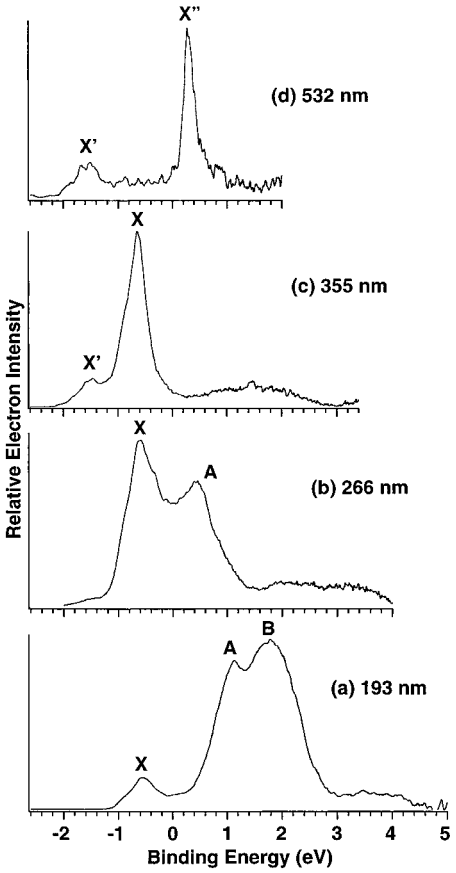

Figure 2. Photoelectron spectra of $[CuPc(SO_3)_4]^{4-}$ at (a) 193, (b) 266, (c) 355, and (d) 532 nm.

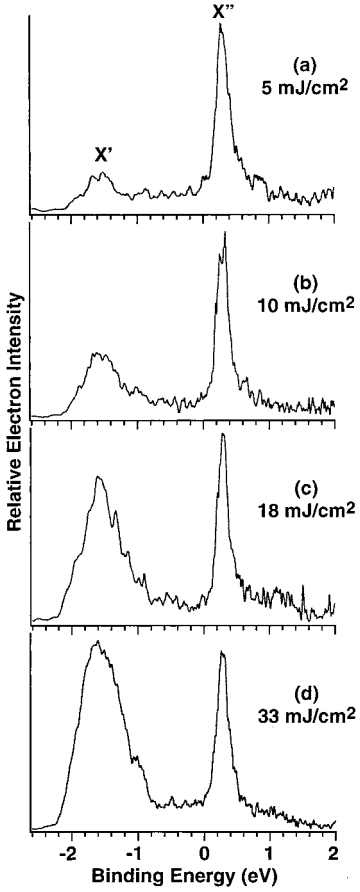

Figure 3. Photon flux-dependent photoelectron spectra of $[CuPc(SO_3)_4]^{4-}$ at 532 nm.

due to detachment of the product dianion by the absorption of a second photon, similar to the weak signals at the high BE side in Figure 2 for the tetraanion. Feature A also almost disappeared completely in the 266 nm spectrum. At 355 nm, feature X was partially observed, being cutoff at the high BE side. Surprisingly, a strong feature (X″) peaking at ∼2.3 eV was observed in the 355 nm spectrum. The X″ feature seemed to be similar to the X″ feature observed in the 532 nm spectrum of the tetraanion (Figure 2d) except that it was much broader in the trianion. A weak low-BE feature (X′) was also observed in the 355 nm spectrum, again similar to the X′ feature observed in the 355 nm spectrum of the tetraanion (Figure 2c). We also tried to take the spectrum of the monosodiumated trianion at 532 nm, but almost no photoelectron signals were observed.

3.3. $[CuPc(SO_3)_4H]^{3-}$. Figure 5 shows the PES spectra of $[CuPc(SO_3)_4H]^{3-}$ at three photon energies. The photon energy dependence of the monoprotonated trianion was nearly identical to that of the monosodiumated species. Again, at 266 nm, feature B completely disappeared and only a lower energy tail was observed for feature A. At 355 nm, the X feature was observed but appeared to become broadened and cutoff at the high-BE side. A very broad feature (X″) was observed at the higher-BE side (Figure 5c), similar to the X″ feature in Figure 4c, but much broader. Again, a weak low-energy feature (X′) was observed in the 355 nm spectrum. At 532 nm, there were also almost no photoelectron signals for the monoprotonated trianion.

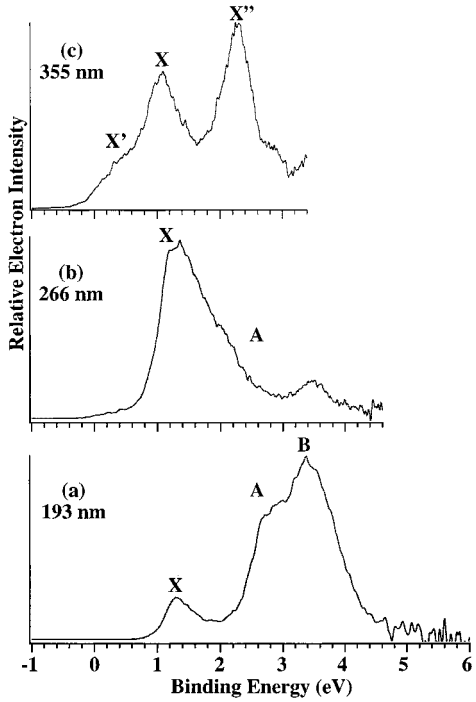

Figure 4. Photoelectron spectra of $[CuPc(SO_3)_4Na]^{3-}$ at (a) 193, (b) 266, and (c) 355 nm.

4. Discussion

4.1. Tuning the Energy Levels of CuPc by Charging. The observation of the negative binding energy feature in the PES spectra of $[CuPc(SO_3)_4]^{4-}$ is remarkable, indicating that the tetraanion is unbound against an electron loss. The photoelectron kinetic energy corresponding to the negative binding energy feature was ∼7.32 eV at 193 nm, i.e., 0.9 eV higher than the photon energy. We noted that the PES spectral features for all three multiply charged anions are rather similar, as shown in

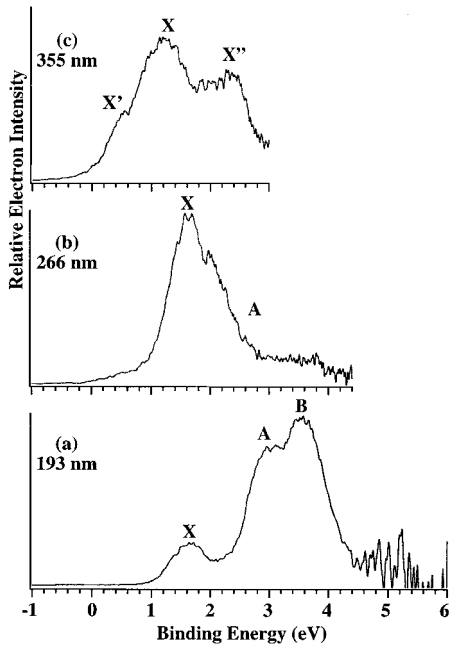

Figure 5. Photoelectron spectra of $[CuPc(SO_3)_4H]^{3-}$ at (a) 193, (b) 266, and (c) 355 nm.

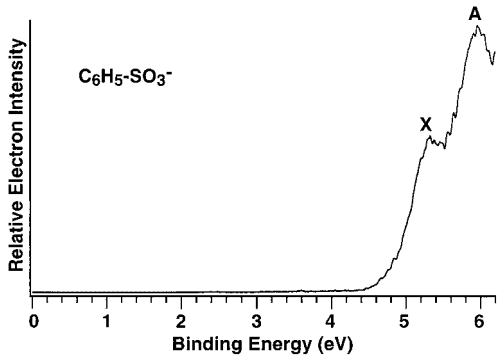

Figure 6. Photoelectron spectrum of $C_6H_5-SO_3^-$ at 193 nm.

Figure 1. There is also a remarkable similarity between these spectra and that of the neutral parent CuPc molecule in the vapor phase except that the neutral CuPc has a much higher BE with an ionization potential (IP) of 6.3 eV.[23] The similarity between the PES spectra of the present charged species and that of the parent CuPc suggests that detachment occurs from MO's containing largely CuPc characters in the tetra- and trianions. This may be understood from the localized nature of the $-SO_3^-$ groups and the electrostatic effects within the charged molecular anions.

Our PES spectra of benzene sulfonate anion ($C_6H_5-SO_3^-$, Figure 6) and other singly charged sulfonate species show two detachment features from the $-SO_3^-$ group separated by ~0.6 eV with a threshold binding energy of ~5 eV. In the current multiply charged anions, the $-SO_3^-$ groups are expected to be localized and act simply as charge carriers. The electron binding energy of $-SO_3^-$ is then expected to be reduced due to the Coulomb repulsion from the other negative charges. Figure 7 shows a schematic molecular structure of the tetraanion and the estimated distances between the charge centers and between the central Cu atom and the charge centers.[24] The $-SO_3^-$ group at position 1 experiences the largest Coulomb repulsion, which amounts to ~3.8 eV ($\sum_{n=2}^{4} e^2/R_{1n}$). Therefore, electrons on this $-SO_3^-$ group are still expected to be bound by at least 1.2 eV (5 eV − 3.8 eV) and the negative BE feature (X) in the PES

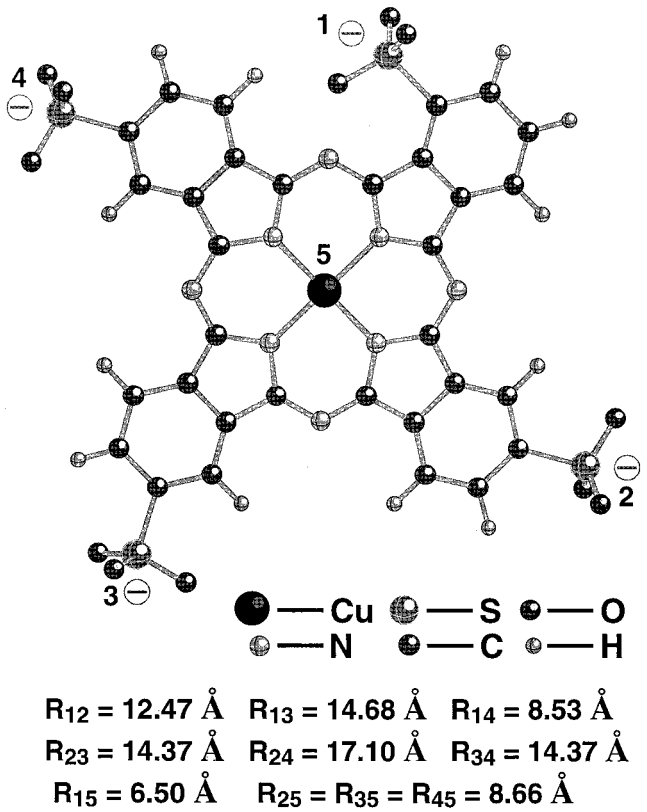

Figure 7. Structure of the $[CuPc(SO_3)_4]^{4-}$ tetraanion as determined in bulk crystals (ref 24), showing the location of the charges and the distances between the charge centers and between the charge centers and the central Cu atom. Our optimization with PCSpartan 5.1 gives similar structural parameters.

spectra of the tetraanion cannot be due to detachment from SO_3-based MO's. However, the four negative charges create a 7.2 eV ($\sum_{n=1}^{4} e^2/R_{n5}$) negative potential on the central Cu atom, i.e., an electron localized on Cu would experience a Coulomb repulsion of ~7.2 eV. Previous density functional theory (DFT) calculations predicted that the HOMO of CuPc is a Cu d_π orbital with a single occupancy ($11b_{2g}$, Figure 8a).[25] An N p_π orbital ($2a_{1u}$, Figure 8a) is close to the HOMO. As schematically shown in Figure 8c, the HOMO of the CuPc is expected to be shifted up by 7.2 eV, due to the Coulomb repulsion from the four negative charges carried by the peripheral $-SO_3^-$, giving rise to a negative binding energy of −0.9 eV (6.3 eV − 7.2 eV). This estimate is in good agreement with the experimental observation, despite of the approximate nature of the procedure.

In the monoprotonated trianion, the most likely protonation position is to the $-SO_3^-$ group at position 1 (Figure 7 and Figure 8b). The Coulomb repulsion to the central Cu due to the three charges at positions 2, 3, and 4 is now reduced to 5 eV ($\sum_{n=2}^{4} e^2/R_{n5}$). The BE of the HOMO in the trianion is then expected to be ~1.3 eV (6.3 eV − 5 eV), again in excellent agreement with the experimental observation that the monoprotonated trianion has a positive binding energy of 1.2 eV. In the monosodiumated trianion, the Na^+ ion is also likely to bind to the $-SO_3^-$ group at position 1 (Figure 7). Because of its large size, Na^+ cannot shield the negative charge as effectively as the proton, thus yielding a slightly lower binding energy (1.0 eV) for the monosodiumated trianion. Comparing the binding energies and spectral features of the multiply charged anions and the neutral CuPc, we see a clear stepwise and nearly rigid tuning of the energy levels of CuPc due to the charging by the $-SO_3^-$ groups at its periphery.

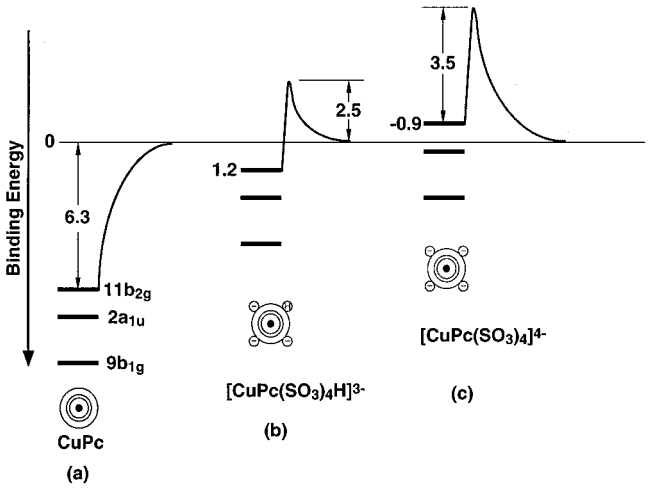

Figure 8. Schematic diagrams showing the top three occupied molecular orbitals of the parent CuPc molecule (a) and the rigid upward shift of these orbitals due to the addition of three (b) and four (c) negative charges. The cartons show the cyclic neutral CuPc molecule and the sequential charging at its periphery. Schematic potential energy curves for removing an electron from the highest occupied orbital of the respective species are shown, illustrating (a) the long range attraction in the CuPc case, (b) the long range Coulomb repulsion and the repulsive Coulomb barrier in the triply charged anion, and (c) both the repulsive Coulomb barrier and the negative electron binding in the quadruply charged anion. The experimentally determined electron binding energies and the repulsive Coulomb barrier heights in electronvolts are indicated. The 6.3 eV ionization potential of CuPc is from ref 23.

4.2. Theoretical Calculations. To confirm the above experimental observations and to further understand the nature of the electronic structures of the charged species, we performed semiempirical theoretical calculations on the parent CuPc, $[CuPc(SO_3)_4H]^{3-}$, and $[CuPc(SO_3)_4]^{4-}$. The calculations were done using the PM3 and PM3(TM) Hamiltonians,[26,27] as implemented in PCSpartan 5.1,[28] for the structural aspect, and the ZINDO/S Hamiltonian for the electronic information.[29] The PM3 Hamiltonians have been shown to provide accurate descriptions of the structural properties for both organic molecules[30] and transition metal complexes.[31] The electrostatic potentials of the three species and their HOMO amplitude plots are shown on the cover and in Figure 9. The electrostatic potentials were evaluated at the optimal geometries and mapped onto the three-dimensional isosurfaces defined by the 0.05 e/au^3 electron probability. The electrostatic potentials show that the negative charges in the tri- and tetraanions are indeed localized on the $-SO_3^-$ groups. The HOMO's of the tri- and tetraanions are similar to that of the parent CuPc and contain little contribution from the $-SO_3^-$ groups, more clearly illustrating the localized nature of the $-SO_3^-$ groups.

Figure 10 shows the MO's of the three species near the HOMO from the current empirical calculations. The one-electron eigenvalues for the MO's of the parent CuPc obtained currently are similar to those obtained previously using DFT.[25] The HOMO is indeed of Cu d_π character, though considerable contributions from the ring system are also observed, as shown on the cover and in Figure 9. The next orbital is an N lone pair, similar to that of Figure 8a. In reality, the top two orbitals are very close in energy and the binding energy of the singly occupied HOMO is underestimated in the current calculation as suggested from the previous DFT calculations.[25] Thus, these energies should only be viewed qualitatively. Nevertheless, the rigid shift of the MO energies due to the $-SO_3^-$ groups is clearly demonstrated. The MO's derived from the $-SO_3^-$ groups (not shown) are more tightly bound, consistent with the above qualitative electrostatic argument. The rigid shifting of the MOs from the calculations confirmed our notion that the $-SO_3^-$ groups are simply charge carriers. They influence the electronic structures of the parent CuPc by purely electrostatic effects.

4.3. Repulsive Coulomb Barriers and Negative Electron Binding. Unlike photoionization of a neutral species (or singly charged anion) where the outgoing electron experiences a long range attractive force (Figure 8a), photoemitted electrons from multiply charged anions experience a long range Coulomb repulsive force. The superposition of the short-range electron binding and the long-range Coulomb repulsion create the RCB against electron loss in multiply charged anions,[7,14,16] as schematically shown in parts b and c of Figure 8. The RCB has been directly observed in photon-energy-dependent PES studies, where photoelectrons may not be observed even when photon energies are higher than the electron binding energies but lower than the RCB.[14−21] This effect is also shown clearly in the photon energy-dependent PES spectra of Figures 2, 4, and 5. We estimated that the current triply and quadruply charged anions possess barrier heights of 2.5 and 3.5 eV, respectively, as given in Figure 8.

Electrons are always bound in a ground state neutral atom or molecule by the Coulomb force due to the positive core. The excess electron in a singly charged anion is also always bound at its ground state. A negative electron binding energy has never been observed before, because it can only exist in multiply charged anions owing to the unique situation of Coulomb repulsion among the excess negative charges and the resulting RCB. As schematically shown in Figure 8 and confirmed in Figure 10 by the theoretical calculations, the negative binding energy observed in $[CuPc(SO_3)_4]^{4-}$ is a direct consequence of the strong intramolecular Coulomb repulsion due to the four excess charges, whereas the triply charged anions still possess positive binding energies because of the reduced intramolecular Coulomb repulsion compared to the quadruply charged anion. The tetraanion is in fact metastable relative to an electron loss and can be viewed to store 0.9 eV purely electrostatic energy.

We tried to estimate the lifetime of the metastable tetraanion with our ion-trap.[16] Surprisingly, we observed no measurable ion loss during a period of 400 s, the longest that we can store the ions. The long lifetime of this metastable tetraanion in the gas phase is remarkable and is attributed to the large barrier height and the large size of the molecule such that the electron has to tunnel a high barrier and a long distance to escape. The RCB can then be viewed as a massive electrostatic corral in this semiplaner molecule, trapping the electron despite its negative binding energy.

4.4. Repulsive Coulomb Barriers and the Photon-Energy-Dependent Photodetachment Spectral Features. Parts a and b of Figure 8 show schematically the RCB for removing an electron from the HOMO of the multiply charged anions. For removing more deeply bound electrons, similar RCB exists. Parts b and c of Figure 8 are essentially initial-state representations of the RCB, or single-particle representations. Spectroscopically, photodetachment processes involve transitions from the ground state of the multiply charged anions to states of an anion with one less charge. The PES features thus represent the energy levels of the lower charge anion, i.e., the final states of the detachment transitions. Parts a and b of Figure 11 show the final state representations of the potential energy curves for the detachment processes of the tetra- and trianions, respectively. The PES spectra of the tetra- and trianions and their photon energy dependence can be understood from these schematic

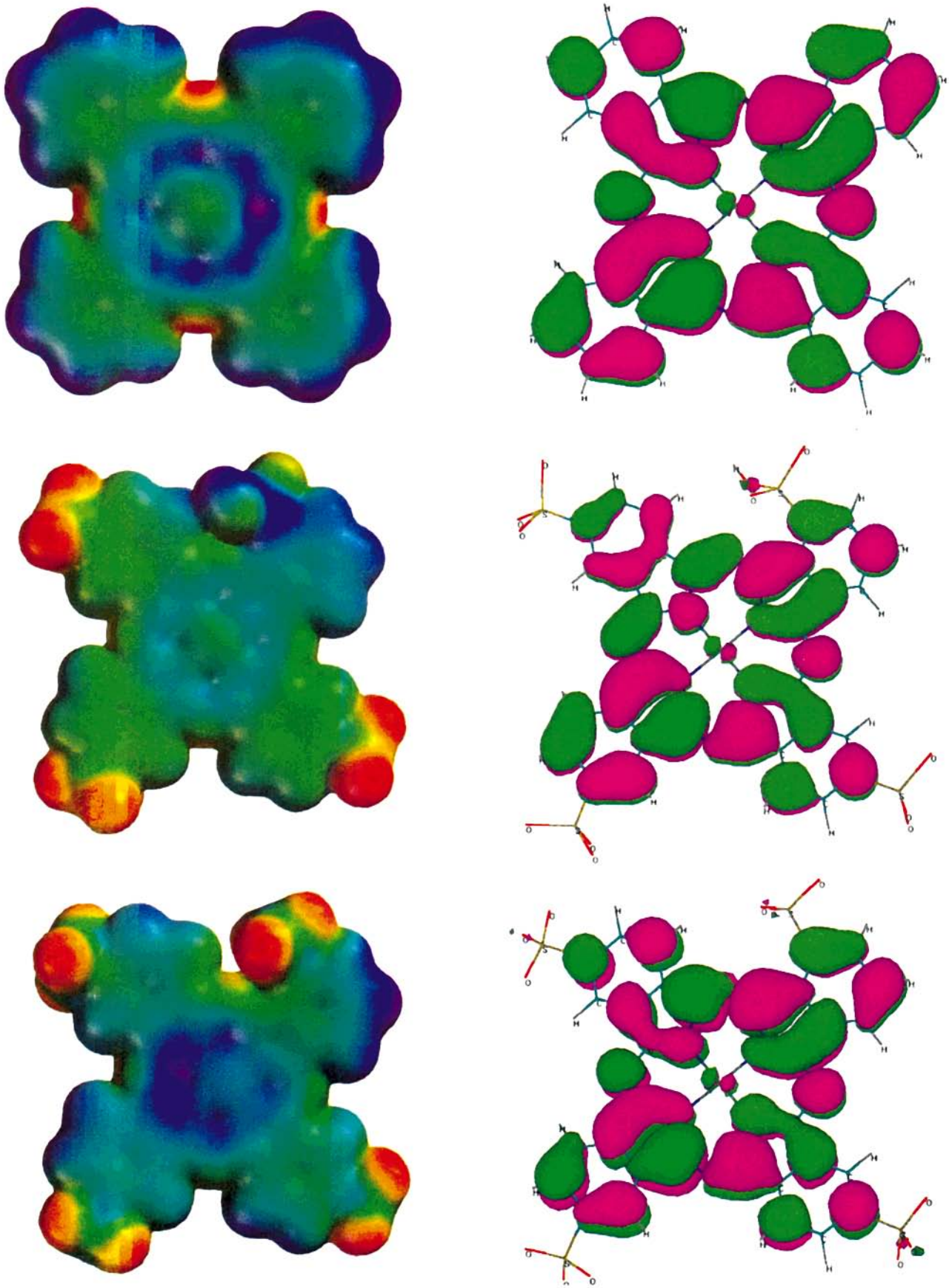

Figure 9. (left column) Electrostatic potentials of CuPc (top), $[CuPc(SO_3)_4H]^{3-}$ (middle), and $[CuPc(SO_3)_4]^{4-}$ (bottom). The electrostatic potential was evaluated at the optimal geometry using PCSpartan 5. 1 (ref 31) and mapped onto the three-dimensional isosurface defined by the 0.05 e/au^3 electron density probability. The scales for the electrostatic potentials from bright to dark colors (kcal/mol): −50 to 15 (top); −220 to −50 (middle); −275 to −125 (bottom). (right column) The HOMO of CuPc (top), $[CuPc(SO_3)_4H]^{3-}$ (middle), and $[CuPc(SO_3)_4]^{4-}$ (bottom).

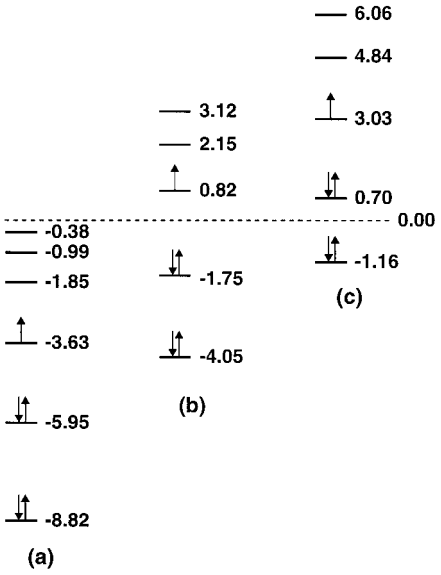

Figure 10. Calculated one-electron eigenvalues (eV) for those molecular orbitals near the highest occupied level, using PCSpartan,[28] for (a) CuPc, (b) $[CuPc(SO_3)_4H]^{3-}$, and (c) $[CuPc(SO_3)_4]^{4-}$, showing the almost rigid shift due to increased charges. Note that the electron binding energies are equal to the negatives of the one-electron eigenvalues, according to the Koopmans' theorem.

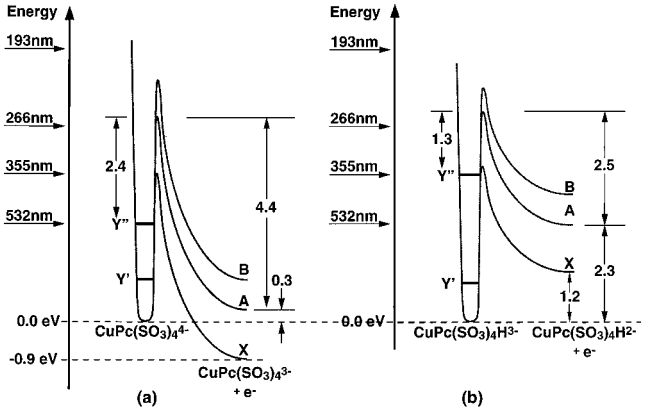

Figure 11. Schematic potential energy curves corresponding to the various detachment channels for (a) $[CuPc(SO_3)_4]^{4-}$ and (b) $[CuPc(SO_3)_4H]^{3-}$. Energetic information and positions of the various photon energies are indicated.

potential energy curves, which illustrate the RCB and the three final states (X, A, and B) observed in the PES spectra. The positions of the four photon energies used are also shown in Figure 11.

Figure 11a shows that the ground state of the trianion $[CuPc(SO_3)_4]^{3-}$ is more stable than the tetraanion $[CuPc(SO_3)_4]^{4-}$, thus the negative binding energy. The photon energy at 193 nm was higher than the RCB of all the three states, X, A, and B; thus, they were all observed. At 266 nm, the photon energy was below the RCB of the B state; thus, the B feature completely disappeared (Figure 2b). The 266 nm photon was also below the RCB of the A state. But it was close enough to the barrier top so that the A state was still partially observed due to electron tunneling.[19] At 355 nm, the photon energy was considerably below the RCB of the A and B states; thus, they completely disappeared and only the X feature was observed. Finally the 532 nm photon was below the RCB of the X, A, and B states, and no signals were observed even though the 532 nm photon was above the asymptotic binding energies of the three states. The RCB of the X state was estimated to be about 3.5 eV, which is also the well depth experienced by the HOMO electron (Figure 11a). This RCB was estimated based on the observation that the 355 nm photon was near the top of the RCB of the X state. The RCB of the A state was estimated to be about 4.4 eV (Figure 11a), based on the observation that the 266 nm photon was just below the top of the RCB of the A state. The RCB of the B state was difficult to estimate and was expected to be similar to that of the A state. The unusual features observed in the 532 nm spectra involved resonant photoabsorption and resonant tunneling and will be discussed in section 4.5.

The PES spectra of the monosodiumated and -protonated trianions (Figures 4 and 5) are nearly identical except that the monosodiumated species has a slightly lower binding energy due to the fact that the Na^+ ion does not shield the negative charge as effectively as the proton. The photon-energy-dependent PES spectra shown in Figures 4 and 5 can be understood from the schematic potential energy curves of Figure 11b, which shows the RCB for the three final states (X, A, and B) for the monoprotonated species and the positions of the four photon energies. Similar to the tetraanion case, the 193 nm photon was above the RCB of all the three states, which thus were all observed at this photon energy. The 266 nm photon was below the RCB of the A and B states (Figure 11b); thus, the B feature completely disappeared in the 266 nm spectra. Since the 266 nm photon was close to the top of the RCB of the A state, a tail of the A feature was still observed due to electron tunneling.[19] The 355 nm photon was slightly below the RCB of the X state, which was partially observed due to tunneling. The X″ feature at 355 nm involved resonant tunneling similar to that observed in the 532 nm spectra of the tetraanions and will be discussed below. The RCB of the X, A, and B states in the trianions was estimated to be about 2.5 eV based on the photon-energy-dependent detachment features. The 532 nm photon was considerably below the RCB of all the three final states in the trianions and no photoelectron signals were expected except through electron tunnelings.[19] Indeed, experimentally almost no photoelectron signals were observed at 532 nm for the two trianions.

4.5. Excited States of Multiply Charged Anions and Resonant Tunneling. What was the nature of the X′ and X″ features observed at 532 nm for the tetraanion (Figure 2d)? Since the 532 nm photon was considerably below the RCB of any of the three states, there were two possible mechanisms for the observed electron signals, either due to a resonant tunneling or a two-photon (multiphoton) process. The photon-flux dependence study (Figure 3) suggested that the X′ feature was due to a two-photon process. The X′ feature occurred at a BE about 1.1 eV lower than the ground state feature (X), suggesting that the detachment transition took place from an initially excited electronic state of the tetraanion at ∼1.1 eV above the ground state, as schematically shown in Figure 11a (Y′). The two-photon nature of this detachment transition implied that the Y′ excited state of the tetraanion was probably produced by an initial photoabsorption of a 532 nm photon to an excited state (Y″ in Figure 11a) and then a relaxation from Y″ to Y′.

The assumed excited state (Y″) should then be ∼2.3 eV (532 nm) above the ground state of the tetraanion. A tetraanion excited to the presumed Y″ state could also undergo an electron tunneling, which would be more effective because the Y″ state is closer to the barrier top. We attributed the sharp and surprising detachment feature (X″) at 0.30 eV (Figure 2d) to such a tunneling process. We call this tunneling process a "resonant tunneling", which is a one-proton process caused by the resonant absorption of a detachment photon by the anion at an appropriate

wavelength. This is similar to an autodetachment process, with one major difference, in that, the resonant tunneling state would be expected to have much longer lifetime because of the RCB. The photon-flux dependence of the X″ feature suggested that it was due to a one-photon process, consistent with the resonant tunneling mechanism.

The 0.30 eV binding energy of the X″-feature corresponded to the threshold BE of the A state, implying that the excited state (Y″) can only couple to the A state of the product trianion. The latter, in turn, suggests that the initial resonant absorption probably involved excitation of the same electron corresponding to the detachment channel A. However, the sharpness of the resonant tunneling feature was still rather puzzling. It was probably due to the long lifetime of the excited state Y″, which was estimated to be ~2.4 eV below the barrier top to the A state as shown in Figure 11a. At such a distance from the top of the RCB, the tunneling probability would have been negligible without the long-lived excited state. It is conceivable that because of the long lifetime of the Y″ excited state the initially populated vibrational excitations by the resonant photoabsorption were relaxed. Thus, tunneling would only proceed from the ground vibrational level of the Y″ intermediate state, giving rise to the sharp tunneling feature. The sharpness of the X″ feature would then suggest that the geometry of the Y″ excited state of the tetraanion and that of the A state of the product trianion are similar. This is consistent with the assumption that both states involved excitations of the same electron.

The long lifetime of the Y″ excited state also suggested that a second photon could be absorbed from this excited state as well. Such a two-photon process would produce a detachment feature about 2.3 eV (the photon energy of 532 nm) to the left of the X″ feature. Such a two-photon feature would then overlap with the X′ detachment feature. In fact, we suspected that at high photon fluxes the X′ feature might indeed have a large contribution from such a two-photon process. It is important to point out that the latter two-photon process would lead to the A state, whereas the two-photon process involving the Y′ state would lead to the ground state (X). We noted that the X′ detachment feature was also observed at 355 nm (Figure 2c) with noticeable intensity, possibly due to a similar two-photon process involving the Y′ state, which would be produced due to a relaxation process following an initial absorption of a 355 nm photon in this case. In fact, the weak features at the high BE side (Figure 2c) could be partly due to a resonant tunneling induced by the absorption of a 355 nm photon. As will be shown below, prominent resonant tunneling effects were indeed observed in the protonated and sodiumated trianions at 355 nm (Figures 4c and 5c).

The 193 and 266 nm spectra of the trianions are discussed in section 4.4 using the potential energy curves schematically shown in Figure 11b. The 355 nm spectra of the two trianions were also similar, both with the surprising appearance of a high (X″) and low (X′) BE feature, which were observed more clearly in the monosodiumated trianion (Figure 4c). The X′ feature was similar to that in the tetraanion (parts c and d of Figure 2) and was likely due to a similar two-photon process, detachment from a Y′ excited state (Figure 11b) produced by a relaxation process following an initial absorption of a 355 nm photon. The X″ feature was likely due to a resonant tunneling from the Y″ excited state (Figure 11b) to the A state, similar to the resonant tunneling at 532 nm in the tetraanion (Figure 2d). The resonant tunneling features in the trianions (X″, Figures 4c and 5c) were much broader than that in the tetraanion, probably due to the fact that the tunneling was more efficient in the trianions. In other word, the Y″ excited state in the trianions was expected to have a short tunneling lifetime because it was much closer to the top of the RCB of the A state (~1.3 eV, Figure 11b). As discussed above, the trianions and the tetraanion have similar occupied energy-level structures. Thus, it was reasonable that the trianions should also have similar excited states as that of the tetraanion, giving rise to similar resonant photoabsorption and resonant tunnelings.

Finally, we should emphasize that the above interpretation of the appearance of the unexpected PES features (X′ and X″) should be viewed as tentative because the energy levels of these multiply charged anions are not known in the gas phase. On the other hand, based on the rich spectroscopy of CuPc as studied extensively in solution,[32,33] existence of low-lying excited states in the gas phase is understandable.

4.6. Relevance of the Current Observations to Other Effects. The anions with negative electron binding energies can be viewed as an electrostatic energy storage medium in the gas phase or a molecular capacitor. They can also be considered as a molecular analogue of a bulk charged metal surface, where the work function combined with the electric field around the metal surface creates a potential barrier (Schottky effect),[34] similar to that shown in Figure 8c. The RCB in multiply charged anions is analogous to the Coulomb barrier experienced in the α-decay of radioactive nuclei,[35] although the distance and length scales are quite different. Similar repulsive Coulomb barriers exist against molecular fragmentations (that result in charge separation, i.e., Coulomb explosion) in multiply charged molecular ions (both anions[7,9,36] and cations[37−40]) and provide dynamic stability to the multiply charged species. Finally, the current observation of tuning molecular energy levels by charging may also be relevant to the interactions of intense laser fields with atomic and molecular systems, leading to tunnel ionization.[41−43] In the latter, the strong electric field induced by a high-power laser suppresses the Coulomb barrier for ionization such that the electron can tunnel out (ionized). In the current tetraanion case, the four extra charges create a negative potential which is effectively higher than the ionization potential of the parent neutral CuPc. Despite the static nature of the electronic interactions in multiply charged anions, the analogy between the two phenomena is interesting and may deserve further considerations.

5. Conclusions

We report photodetachment photoelectron spectra of a quadruply charged anion, $[CuPc(SO_3)_4]^{4-}$, and its monoprotonated and -sodiumated trianions, $[CuPc(SO_3)_4H]^{3-}$ and $[CuPc(SO_3)_4Na]^{3-}$ in the gas phase. A negative electron binding energy was observed in the tetraanion, which was found to be a long-lived metastable species against an electron loss with a negative electron binding energy of −0.9 eV. The tetraanion can thus be viewed as a molecular capacitor storing 0.9 eV electrostatic energy. The lifetime of this anion was estimated to be >400 s. The long lifetime of this metastable anion is due to the large magnitude of the repulsive Coulomb barrier, characteristic of multiply charged anions, that acts as a sort of electrostatic corral trapping the negatively bounded electron against autodetachment.

We observed that the PES spectral features of the charged species are similar to that of the parent neutral CuPc molecules and thus found a stepwise tuning of the CuPc molecular energy levels due to charging. Semiempirical calculations were carried out for the neutral CuPc and the tri- and tetraanions and showed a rigid upward shifting of the molecular orbitals of the CuPc

due to the peripheral charges carried by the $-SO_3^-$ groups. The charges are mainly localized on the $-SO_3^-$ groups, which have little mixing with the HOMO of the parent molecule (see Figure 9) and only exert an electrostatic effect. This is the first direct observation of the influence of a distant charge on the electronic energy levels of a molecule. Resonant tunneling through the repulsive Coulomb barriers, due to excited states of the parent anions, was also observed in all the three multiply charged anions. The CuPc species exhibit rich spectroscopies and would deserve further investigations. Studies using tunable lasers would be very interesting and may uncover more excited states and resonant tunneling effects.

Acknowledgment. This work is supported by The U.S. Department of Energy, Office of Basic Energy Sciences, Chemical Science Division. Acknowledgment is also made to the donors of the Petroleum Research Fund, administered by the American Chemical Society, for partial support of this research. This research was performed at the W. R. Wiley Environmental Molecular Sciences Laboratory, a national scientific user facility sponsored by DOE's Office of Biological and Environmental Research and located at Pacific Northwest National Laboratory, which is operated for DOE by Battelle under Contract DE-AC06-76RLO 1830. L.S.W. is an Alfred P. Sloan Foundation Research Fellow.

References and Notes

(1) Honig, B.; Nicholls, A. *Science* **1995**, *268*, 1144.
(2) Stephens, P. J.; Jollie, D. R.; Warshel, A. *Chem. Rev.* **1996**, *96*, 2491.
(3) Rockwood, A. L.; Busman, M.; Smith, R. D. *Int. J. Mass Spectrom. Ion Processes* **1991**, *111*, 103.
(4) Gross, D. S.; Williams, E. R. *J. Am. Chem. Soc*. **1995**, *117*, 883.
(5) Schnier, P. D.; Gross, D. S.; Williams, E. R. *J. Am. Chem. Soc*. **1995**, *117*, 6747.
(6) Gronert, S. *Int. J. Mass Spectrom.* **1999**, *185*, 351.
(7) Scheller, M. K.; Compton, R. N.; Cederbaum, L. S. *Science* **1995**, *270*, 1160. Dreuw, A.; Sommerfeld, T.; Cederbaum, L. S. *J. Chem. Phys.* **1998**, *109*, 2727.
(8) Kalcher, J.; Sax, A. F. *Chem. Rev.* **1994**, *94*, 2291.
(9) Boldyrev, A. I.; Gutowski, M.; Simons, J. *Acc. Chem. Res.* **1996**, *29*, 487. Gutsev, G. L.; Boldyrev, A. I. *J. Phys. Chem.* **1990**, *94*, 2256. Enlow, M.; Ortiz, J. V.; Luthi, H. P. *Mol. Phys.* **1997**, *92*, 441.
(10) Freeman, G. R.; March, N. H. *J. Phys. Chem.* **1996**, *100*, 4331.
(11) Blades, A. T.; Klassen, J. S.; Kebarle, P. *J. Am. Chem. Soc.* **1995**, *117*, 10563.
(12) Blades, A. T.; Ho, Y.; Kebarle, P. *J. Phys. Chem.* **1996**, *100*, 2443.
(13) Compton, R. N.; Tuinman, A.; Klots, C. E.; Pederson, M. R.; Patton, D. C. *Phys. Rev. Lett.* **1997**, *78*, 4367.
(14) Wang, X. B.; Ding, C. F.; Wang, L. S. *Phys. Rev. Lett*. **1998**, *81*, 3351.
(15) Wang, L. S.; Ding, C. F.; Wang, X. B.; Barlow, S. E. *Rev. Sci. Instrum*. **1999**, *70*, 1957.
(16) Wang, L. S.; Ding, C. F.; Wang, X. B.; Nicholas, J. B. *Phys. Rev. Lett.* **1998**, *81*, 2667.
(17) Ding, C. F.; Wang, X. B.; Wang, L. S. *J. Chem. Phys*. **1999**, *110*, 3635.
(18) Wang, X. B.; Ding, C. F.; Nicholas, J. B.; Dixon, D. A.; Wang, L. S. *J. Phys. Chem. A* **1999**, *103*, 3423.
(19) Wang, X. B.; Ding, C. F.; Wang, L. S. *Chem. Phys. Lett*. **1999**, *307*, 391.
(20) Ding, C. F.; Wang, X. B.; Wang, L. S. *J. Phys. Chem. A* **1998**, *102*, 8633.
(21) Wang, X. B.; Wang, L. S. *Nature* **1999**, *400*, 245.
(22) Yamashita, M.; Fenn, J. B. *J. Phys. Chem.* **1984**, *88*, 4451, 4671.
(23) Berkowitz, J. *J. Chem. Phys.* **1979**, *70*, 2819.
(24) Brown, C. J. *J. Chem. Soc. A* **1968**, 2488.
(25) Rosa, A.; Baerends, E. J. *Inorg. Chem*. **1994**, *33*, 584.
(26) Stewart, J. J. *J. Comput. Chem*. **1989**, *10*, 221. Stewart, J. J. *J. Computer-Aided Mol. Des.* **1990**, *6*, 69.
(27) Yu, J.; Adei, E.; Hehre, W. J. Unpublished.
(28) *PC Spartan Plus 5.1*; Wavefunction, Inc., Von Carman Ave., Irvine, CA 92612.
(29) Ridley, J. E.; Zerner, M. C. *Theor. Chim. Acta* **1976**, *42*, 223. Bacon, A. D.; Zerner, M. C. *Theor. Chim. Acta* **1979**, *53*, 21.
(30) Kurtz, H. A.; Stewart, J. J.; Dieter, K. M. *J. Comput. Chem*. **1990**, *11*, 82.
(31) *PC Spartan Plus User's Guide*; Wavefunction, Inc.: Irvine, CA, 1997; Section 13.
(32) Thomas, A. L. *Phthalocyanine Research and Applications*; CRC Press: Boca Raton, 1990.
(33) Leznoff, C. C.; Lever, A. B. P., Ed. *Phthalocyanines: Properties and Applications*; VCH: New York, 1989.
(34) D'Haennens, I. J. In *Encyclopedia of Physics*; Lerner, R. G., Trigg, G. L., Eds.; VCH: New York, 1991; pp 1251−1253.
(35) See, for example: Hodgson, P. E.; Gadioli, E.; Erba, E. G. *Introductory Nuclear Physics*; Clarendon Press: Oxford, 1997.
(36) Weikert, H. G.; Cederbaum, L. S.; Tarantelli, F.; Boldyrev, A. I. *Z. Phys. D* **1991**, *18*, 299.
(37) Vekey, K. *Mass Spectrom. Rev.* **1995**, *14*, 195.
(38) Nefedova, V. V.; Boldyrev, A. I.; Simons, *J. Int. J. Quantum Chem*. **1995**, *55*, 441.
(39) Brechignac, C.; Cahuzac, P.; Kebaili, N.; Leygnier, J. *Phys. Rev. Lett.* **1998**, *81*, 4612.
(40) Schroder, D.; Harvey, J. N.; Schwarz, H. *J. Phys. Chem. A* **1998**, *102*, 3639.
(41) Ilkov, F. A.; Decker, J. E.; Chin, S. L. *J. Phys. B* **1992**, *25*, 4005.
(42) Walsh, T. D. G.; Ilkov, F. A.; Decker, J. E.; Chin, S. L. *J. Phys. B* **1994**, *27*, 3767.
(43) DeWitt, M. J.; Levis, R. J. *J. Chem. Phys*. **1995**, *102*, 8670.